JOURNAL OF Materials CHEMISTRY

Crystallization behaviour of the series of solid solutions $Zr_xTi_{1-x}O_2$ and $Pb_yZr_xTi_{1-x}O_{2+y}$ prepared by the sol–gel process

Rotraut Merkle* and Helmut Bertagnolli

Institut für Physikalische Chemie, Universität Stuttgart, Pfaffenwaldring 55, D-70550 Stuttgart, Germany

Received 16th June 1998, Accepted 11th August 1998

A series of solid solutions of zirconium titanium oxide $Zr_xTi_{1-x}O_2$ ($0 \leqslant x \leqslant 1$) and $Pb_yZr_xTi_{1-x}O_{2+y}$ ($0 \leqslant y \leqslant 1.15$, $0 \leqslant x \leqslant 1$) up to lead zirconate titanate $PbZr_xTi_{1-x}O_3$ was prepared from zirconium and titanium *n*-propoxide and lead acetate, dissolved in 2-methoxyethanol, by the sol–gel process. The crystallization was investigated by differential thermal analysis (DTA), and the apparent activation energies, crystallization enthalpies and Avrami exponents were determined. The crystalline phases were identified by X-ray diffraction (XRD). Within the series of solid solutions $Zr_xTi_{1-x}O_2$, the activation energy changes from *ca.* 200 kJ mol^{-1} for samples with low ($x \leqslant 0.14$) or high ($x \geqslant 0.9$) ZrO_2 content, to *ca.* 800 kJ mol^{-1} for intermediate ZrO_2 contents. Within the series of solid solutions $Pb_yZr_xTi_{1-x}O_{2+y}$, PbO lowers the activation energies and hinders the crystallite growth.

1 Introduction

The sol–gel process allows the simple preparation of oxidic solid solutions with a continuous variation of the stoichiometry and a homogeneous distribution of all components at the molecular level. It is frequently used for the synthesis of electrical and magnetic ceramics with optimized properties.[1] Owing to the high homogeneity of the amorphous oxide mixture which is the product of the pyrolysis of the dried gels, crystallization can occur without long range diffusion at moderate temperatures. Thus, desired or undesired metastable phases can be the first crystallization products[2] which transform to the thermodynamically stable structures at higher temperatures.

In the first step, the binary system of $Zr_xTi_{1-x}O_2$ [ZT(X) with $X = 100x =$ content of ZrO_2 in %] prepared by the sol–gel process is investigated to study the effect of substituting Zr by Ti on the crystallization behaviour. Zr and Ti can be interchanged easily in many ternary systems, *e.g.* in the perovskites ABO_3 on the B sites with A = Pb, Ba or Sr. Nevertheless, in the binary system ZrO_2–TiO_2 the differences between zirconium and titanium may have larger effects. The hydrolysis of Ti—OR groups and the condensation of Ti—OH groups are faster than the corresponding reactions of Zr—OR and Zr—OH groups.[3–5] While titanium is mostly octahedrally coordinated by oxygen, zirconium prefers larger coordination numbers of 7 to 8.

In the second step, the PbO content in the ternary system $Pb_yZr_xTi_{1-x}O_{2+y}$ [P(Y)ZT(X) with $Y = 100y =$ content of PbO in %] is varied at fixed ZrO_2 content X, and gives a series of solid solutions, extending from P(Y)T, P(Y)ZT(45) to P(Y)Z. Between ZrO_2 and PZ, a complete series of solid solution can be prepared by coprecipitation,[6] where the structure changes from the tetragonally distorted fluorite structure for the lead poor samples to the pyrochlore structure for lead rich samples. The P(Y)ZT(X) series provides information about the role of the lead in the crystallization process. The knowledge obtained from all these series can improve the understanding of the crystallization of PZT prepared by the sol–gel process.

2 Experimental

The samples ZT(X) with $0 \leqslant X \leqslant 100\%$ were prepared from a 1 molar solution of Zr/Ti *n*-propoxide [$Zr(OPr^n)_4$ 70 wt% solution in Pr^nOH, $Ti(OPr^n)_4$ 98 wt% solution in Pr^nOH, Alfa] in 2-methoxyethanol (MOE, distilled before use). During the addition of 5 mol H_2O per mol Zr/Ti, a slightly turbid gel was formed. It was dried at 90 °C, 20 mbar and crushed to a fine powder. For gels containing more than 10% ZrO_2, a steam treatment[7] was applied to prevent the formation of carbon residues during pyrolysis which severely disturb the following DTA measurements. For gels with a ZrO_2 content of up to 10% the steam treatment cannot be applied because small anatase crystallites are formed during this treatment.

Additionally, the solvent was varied and samples of ZT(X) were prepared with *n*-propanol (PrOH, distilled before use) instead of MOE. During hydrolysis, a voluminous precipitate instead of a gel was formed. It was dried under the same conditions as the gel samples. These samples pyrolyze without any formation of carbon residues even without steam treatment. Samples of ZT(X) prepared in PrOH with and without steam treatment [labeled ZT(X)-PS and ZT(X)-P] are examined to study the effect of the steam treatment on the crystallization.

Lead containing samples were prepared analogously to ZT(X) by dissolving appropriate amounts of lead acetate trihydrate (99.5%, Fluka) in methoxyethanol (100 ml per 0.1 mol of Zr/Ti alkoxide), adding Zr/Ti *n*-propoxide and hydrolyzing. After the steam treatment, samples of P(Y)ZT(45) with $0 \leqslant Y \leqslant 115\%$ pyrolyze without carbon residues. In the series P(Y)Z, samples with a PbO content larger than 10% form carbon residues and cannot be studied further. Samples of P(Y)T must be prepared in *n*-propanol (with anhydrous lead acetate to prevent precipitation before hydrolysis) without steam treatment, because they crystallize during the course of the steam treatment, and P(Y)T, prepared in MOE without steam treatment, forms carbon residues. Samples of P(Y)T-P with $Y > 15\%$ crystallize in a different structure ($PbTi_3O_7$) and were not examined further.

A Netzsch STA 409 with Al_2O_3 crucibles was used for DTA measurements. The mass of the samples was 5–30 mg, the furnace was purged with 0.5 l min^{-1} of dry air. All samples show an exothermic DTA peak at about 300 °C due to the pyrolysis of the organic components, and a total weight loss of less than 10% for ZT(X) up to about 25% for PZT(X). After this pyrolysis step, no further weight loss occurs, which indicates that the samples have reached the final composition and contain no further organic residues. Activation energies were determined from DTA runs with heating rates from

1 K min^{-1} to 30 K min^{-1}. Crystallization enthalpies were calculated from the integrals of the DTA peaks. Some samples have extremely narrow DTA peaks. Thus the total crystallization heat is liberated in a very short time, and the sample is overheated which also accelerates the crystallization. This leads to unrealistically high values of the Avrami exponents determined from the DTA peak shape. Therefore the samples were mixed with Al_2O_3 as an inert material in the mass ratio of 1:2 for determining Avrami exponents from the DTA peak shape.

X-Ray diffractograms were measured on a horizontal Stoe Stadi P diffractometer with a focussing germanium monochromator and a curved position sensitive detector (PSD). Cu-Kα radiation (40 kV, 35 mA) was used. The samples were pressed to tablets, fixed on a rotating sample holder and measured in reflection mode. The measured intensities were corrected for absorption[8] and polarization.[9] The crystallite size L was determined from the full width at half maximum (FWHM) $\delta(\kappa)$ of the reflections on the κ scale [$\kappa = 4\pi \sin(\Theta)/\lambda$] with the Scherrer equation[10] $L = 2\pi/\delta(\kappa)$. The measured $\delta(\kappa)_{exp}$ was corrected for apparatus broadening $\delta(\kappa)_{app}$ according to[11] $\delta(\kappa) = \delta(\kappa)_{exp} - \delta(\kappa)_{app}$ with the assumption that the peak shapes are lorentzian. The apparatus broadening $\delta(\kappa)_{app}$ was determined from sintered PT and PZ samples with sufficiently large crystallite size so that $\delta(\kappa)_{exp}$ equals $\delta(\kappa)_{app}$.

Diffractograms of samples heated to 350 °C, where the pyrolysis of organic components is completed, prove that these samples are amorphous. Diffractograms of samples heated above the temperatures of the crystallization peaks, which were observed in the DTA measurements, show the complete transformation to the crystalline phases.

3 Crystallization kinetics

The isothermal formation of a crystalline phase from an amorphous or another crystalline phase by a mechanism of nucleation and surface controlled growth can be described by the Johnson–Mehl–Avrami equation:[12–15]

$$1 - \chi(t) = \exp(-apk^m t^n/m) \quad (1)$$

$\chi(t)$ is the fraction transformed at time t, m is the dimensionality of the growth and $n = m$ for a constant number of nuclei, and $n = m + 1$ for a constant nucleation rate; a includes a geometry factor and the reciprocal of the molar volume; p and k are the rate constants of nucleation and linear crystallite growth. They are assumed to follow an Arrhenius law:

$$p = p_0 \exp(-E_n/RT) \quad (2)$$

$$k = k_0 \exp(-E_g/RT) \quad (3)$$

The Kissinger plot[16,17] which was deduced in order to determine the activation energy of a simple, not interface controlled reaction from the dependence of the shift of the DTA peak maximum temperature T_m from the heating rate α, can also be applied to crystallization processes obeying Avrami kinetics. The plot of $\ln(\alpha/T^2_m)$ *versus* $1/T_m$ yields an apparent activation energy E_a' as the weighted average of E_n and E_g:

$$E_a' = \frac{E_n + mE_g}{n} \quad (4)$$

For the crystallization of ZT(X) and P(Y)ZT(X) samples, both the nucleation (*i.e.* the growth of a subcritical nucleus to a supercritical nucleus) and the crystallite growth require the reorientation of the (Zr/Ti)O_6 network by breaking and reconstructing (Zr/Ti)—O—(Zr/Ti) bonds. Therefore, it is very likely that $E_n \approx E_g$ and thus $E'_\alpha \approx E_n \approx E_g$. In this case, the crystallization is isokinetic,[18,19] and the following relation holds for the intercept b of the Kissinger plot and the preexponential factors p_0, k_0:

$$b - \ln \frac{R}{E_a'} \approx \frac{1}{n} \ln \frac{ap_0 k_0^m}{m} = \ln c_0' \quad (5)$$

The molar volume contained in a can be estimated from the volume of the unit cell, which is usually of the order of some Å^3, and the geometry factor included in a is of the same order of magnitude as m, thus the apparent preexponential factor c_0' approximately equals the geometrical average of the preexponential factor of the nucleation rate per molecular unit $p_0' = p_0/N_A$ and of the growth rate k_0:

$$c_0' \approx (p_0' k_0^m)^{1/n} \quad (6)$$

An approximate value n^{Gr} of the Avrami exponent n can be determined from the integral $\int h(T)\mathrm{d}T$ and the maximum height $h(T_m)$ of the DTA peak[20] by the phenomenological relation, deduced from simulated DTA curves:

$$n^{Gr} = 0.02 + C \frac{h(T_m) T_m^2}{E_a' \int h(T)\mathrm{d}T} \quad (7)$$

C is 2.211×10^{-4} for energies in eV,[20] corresponding to $C = 0.02133$ for energies in kJ mol^{-1}. For the crystallization of PZT prepared by the sol–gel process,[21] a good agreement was found between n determined from Avrami plots of isothermal crystallization measurements and approximate values of n^{Gr} from non-isothermal DTA measurements.

4 Solid solution series ZT(X)

The crystalline phases formed in the course of the heating of the ZT(X) samples depend on the ZrO_2 content X. The pure TiO_2 and the titanium rich samples up to ZT(18) crystallize in the anatase structure. The formation of this metastable phase by a sol–gel process is also reported for TiO_2 in refs. 22–24.

In the intermediate range of ZT(25) to ZT(60), the samples crystallize in the orthorhombic srilankite structure (α-PbO_2 structure), whose unit cell parameters vary linearly with the ZrO_2 content.[25] At temperatures below about 1200 °C, srilankite $TiZr_2O_6$ is the only stable compound in this stoichiometry range, and above 1200 °C only $ZrTiO_4$ is stable.[26] For the sol–gel samples crystallizing at much lower temperatures, the metastable srilankite is formed over a wide range. The diffractograms of the crystalline phases of ZT(25)–ZT(60) are collected in Fig. 1.

The samples with a ZrO_2 content of more than 60% crystallize mainly in the tetragonally distorted fluorite structure. The formation of this phase in the course of the sol–gel process is also reported for ZrO_2 in ref. 27, although this phase is stable only at temperatures of 1100–2300 °C. The diffractograms of the crystalline phases of ZT(75)–ZrO_2 are also collected in Fig. 1. ZT(75) and ZT(85) still show a very weak srilankite (011) reflection. Shoulders at $2\Theta = 28.2°$ and $2\Theta = 31.5°$ besides the main (111) fluorite reflection indicate the presence of small amounts of the monoclinic ZrO_2 phase formed from the tetragonal phase during pressing of the sample tablet.

Application of the Scherrer equation yields crystallite sizes of about 250 Å for TiO_2 and ZT(10), and over 1000 Å for ZT(18). The crystallite size is in the range 140–350 Å for the srilankite phases, and rises for the fluorite phases to 640 Å for ZT(95) and over 1000 Å for ZrO_2. For the samples prepared in PrOH, the steam treatment has no effect on the crystallite sizes. The only exceptions are TiO_2-P and ZT(10)-P, where the crystallite size increases significantly with the use of PrOH, and reaches about 1000 Å.

The DTA curves of ZT(X), prepared in MOE, are shown in Fig. 2. TiO_2 and ZT(10) crystallize at about 400 °C and 500 °C, respectively. The samples ZT(18)–ZT(75) with moder-

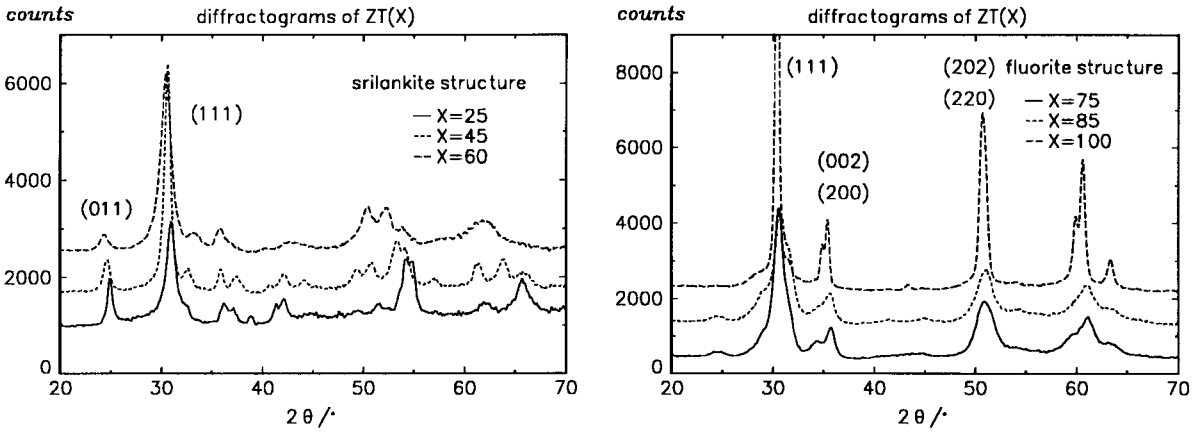

Fig. 1 Diffractograms of the crystalline phases of $Zr_xTi_{1-x}O_2$ [ZT(X) with $X=100x=ZrO_2$ content in %], shifted along the ordinate for clarity.

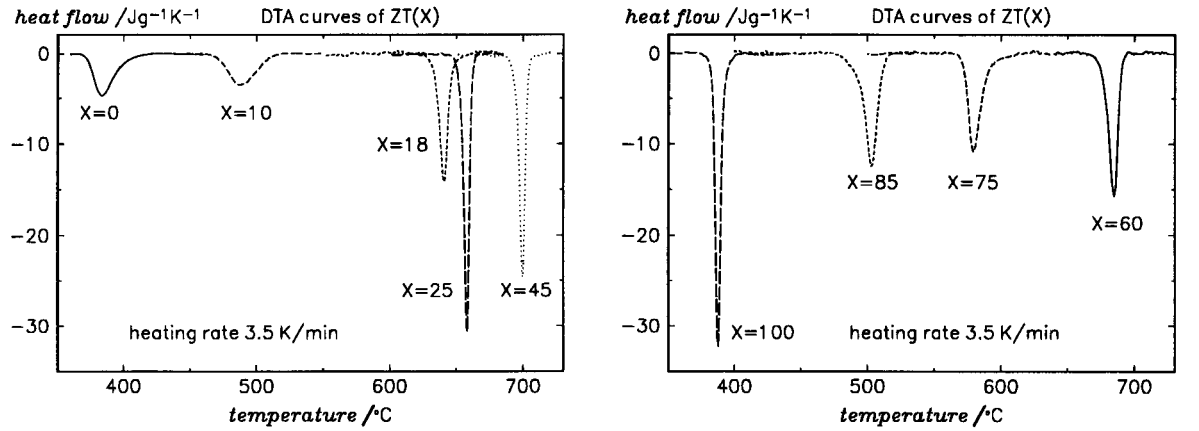

Fig. 2 Differential thermal analysis curves of $Zr_xTi_{1-x}O_2$ [ZT(X) with $X=100x=ZrO_2$ content in %], prepared by a sol–gel process in 2-methoxyethanol.

ate ZrO_2 contents crystallize at temperatures above 650 °C and exhibit very narrow DTA peaks. The crystallization temperature decreases with increasing ZrO_2 content down to about 400 °C for ZrO_2. The crystallization temperature is independent of which crystal structure is formed, because the samples crystallizing above 650 °C crystallize in the anatase [ZT(18)], srilankite [ZT(25)–ZT(60)] and fluorite [ZT(75)] structures. All the crystallization enthalpies are in the range of about 14–18 kJ mol^{-1}; only the samples TiO_2 and ZT(10), prepared in MOE without steam treatment, show lower values of about 10 kJ mol^{-1}.

The apparent activation energies E_a', determined from the Kissinger plots (examples are shown in Fig. 3), are depicted in Fig. 4. They show the same trend as the crystallization temperatures with a distinct maximum at medium ZrO_2 contents. For the samples prepared in MOE, the apparent activation energies of about 800 kJ mol^{-1} reach the values of the sublimation enthalpies of ZrO_2 and TiO_2 (811 kJ mol^{-1} and 695 kJ mol^{-1} [28]). The crystallization behaviour of the samples prepared in PrOH with steam treatment is very similar to that of the samples prepared in MOE with steam treatment. Thus, the different early stages (gel *versus* voluminous precipitate) have no effect on the crystallization. The samples prepared in PrOH without steam treatment show the same general trends in the activation energies, but the maximum values of about 550 kJ mol^{-1} for ZT(18)–ZT(75) are lower than for the steam treated samples.

The drastic change of the apparent activation energies with the zirconium content is not correlated with the changes in the final crystal structures. Therefore the reason for this change must be sought in the amorphous phase or the crystallization process. In the crystallization process, some (Zr/Ti)—O bonds

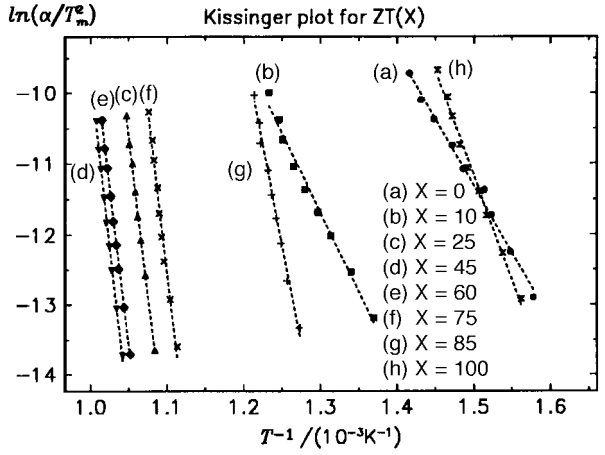

Fig. 3 Kissinger plots of $Zr_xTi_{1-x}O_2$ [ZT(X) with $X=100x=ZrO_2$ content in %], prepared by a sol–gel process in 2-methoxyethanol.

must be broken in order to allow the linked (Zr/Ti)O_6 octahedra to arrange according to the crystal structures. For the pure components ZrO_2 and TiO_2 of the binary system (Zr/Ti)O_2, the activation energies are similarly low at about 200 kJ mol^{-1}. This can be interpreted by the following, simplified model. The Ti—O—Ti bonds (and Zr—O—Zr bonds) can be broken with the same probability in both directions:

$$O-Ti-O-Ti-O \rightarrow O-Ti-\underline{O}| + Ti-O$$

$$O-Ti-O-Ti-O \rightarrow O-Ti + |\underline{O}-Ti-O$$

thus the breaking of one (or very few) Ti—O—Ti connections

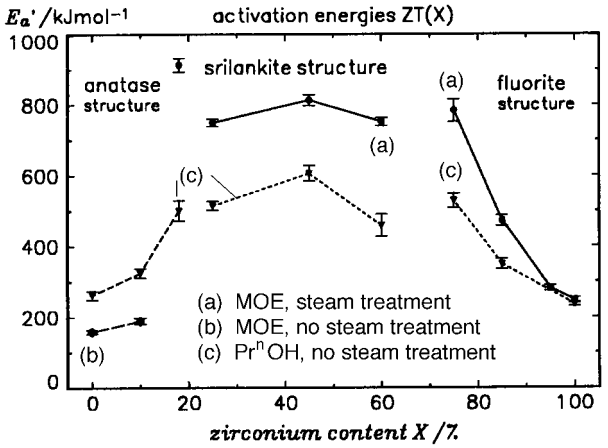

Fig. 4 Apparent activation energies of $Zr_xTi_{1-x}O_2$ [ZT(X) with $X=100x=ZrO_2$ in %], with standard deviation calculated from the linear regression.

yields fragments which are suitable for the progress of the crystallite growth.

E_a' and thus E_n and E_g are drastically increased when more than about 15% of the other metal cation is present. Although Zr and Ti are chemically similar, they disturb each other markedly in the crystallization process. As a consequence of the larger electronegativity and the larger positive charge density of Ti^{4+} compared to Zr^{4+}, the Ti—O—Zr bonds are broken preferably in one direction:

$$-O-Ti-O-Zr-O-\rightarrow -O-Ti-\underline{O}|+Zr-O-$$

Thus mainly the fragments $-O-Ti-\underline{O}|$ and Zr—O— are formed from —O—Ti—O—Zr—O— bonds. If other fragments, *e.g.* —O—Ti or $|\underline{O}-Zr-O-$, are needed for the reconstruction of the $(Zr/\underline{Ti})O_6$ network during the crystallization, additional bonds of a $(Zr/Ti)O_6$ octahedron must be broken, which strongly increases the activation energy. This will happen more often when the number of Ti—O—Zr bonds is high, *i.e.* at intermediate zirconium contents.

In order to estimate the probability of Ti—O—Zr bonds in amorphous samples of ZT(X), the hydrolysis of the zirconium and titanium alkoxides shall be considered briefly. The structural aspects of the formation of oligomers and polymers during the hydrolysis of zirconium and titanium alkoxides were studied extensively by Bradley and coworkers.[29–31] Kinetic aspects of the different steps comprising the complex hydrolysis and condensation reactions were investigated later.[3–5] Owing to the larger charge density of the Ti^{4+}, which makes the hydrogen atoms of coordinated water molecules in Ti—OH_2 more acidic, the hydrolysis of Ti—OR groups to Ti—OH is faster than the hydrolysis of Zr—OR groups.

For the formation of TiO_2 from 0.1–0.2 molar solutions of $Ti(OEt)_4$ in ethanol with a water : Ti ratio of 2–5, a rate law of $\tau=k[H_2O]^3[Ti(OEt)_4]$ (τ is the time from the addition of the water to the first turbidity of the solution) was found.[3] It indicates that the hydrolysis reaction

$$Ti(OR)_4+3H_2O\rightarrow Ti(OR)(OH)_3+3ROH$$

is the rate limiting step, and a value of $k=6.6$ l^4 mol^{-4} s^{-1} was determined for the hydrolysis. In contrast, a rate law of $\tau=k[H_2O][Ti(OEt)_4]^2$ is observed for dilute solutions [0.01–0.03 molar solutions of $Ti(OEt)_4$ in ethanol] with a large excess of water (10–100 mol H_2 per mol Ti).[4] Instantaneous hydrolysis to $Ti(OH)_3(OEt)$ is proved by measuring the rapid decrease of the water content. The formation of precipitates is much slower, and the condensation reaction is the rate-limiting step.

For the hydrolysis of 0.05–0.53 molar solutions of $Zr(OPr^n)_4$ in ethanol, a rate law of $\tau=k'[H_2O]^3[Zr(OPr)_4]$ with $k'=0.9$ l^4 mol^{-4} s^{-1} was found.[5] As the alkoxide exchange reaction $M(OPr^n)+EtOH\rightarrow MOEt+Pr^nOH$ is fast, even at room temperature,[4] it can be assumed that the species which was hydrolyzed was mostly $Zr(OEt)_4$, and therefore k[3] and k'[5] can be compared to prove the faster hydrolysis of titanium alkoxides compared to the corresponding zirconium alkoxides.

The condensation reaction of the Ti—OH groups, which follows the hydrolysis step,

$$Ti-OH+RO-Zr\rightleftharpoons Ti-O-Zr+ROH$$

$$Ti-OH+HO-Ti\rightleftharpoons Ti-O-Ti+H_2O$$

occurs easier with Zr—OR than with Ti—OH due to the larger basicity of the leaving group, and leads to the favoured formation of Ti—O—Zr bonds instead of the homocondensation to Ti—O—Ti and Zr—O—Zr. In an EXAFS study at the Zr K-edge of PZT gel which was not dried,[32] the first metal backscatterer around Zr was found to be Ti, indicating the preferred heterocondensation. Therefore already at moderate ZrO_2 or TiO_2 contents of about 20%, a large amount of Zr—O—Ti bonds may be present and causes the change in the crystallization behaviour.

The Avrami exponents n^{Gr}, determined from the DTA peak shape, show no significant difference between the samples prepared in MOE or PrOH and with or without steam treatment. n^{Gr} of the samples crystallizing in the anatase structure decreases from almost 4 for TiO_2 to about 2 for ZT(18). The samples forming the srilankite phase have Avrami exponents in the range of 3–4. n^{Gr} decreases to $n^{Gr}\approx 2$ for ZT(75) with the change to the fluorite phase, and increases again with increasing ZrO_2 content to about 4 for ZrO_2. The closer the stoichiometry of a sample is to that of the 'pure' phase (TiO_2 with anatase structure, $ZrTi_2O_6$ and $ZrTiO_4$ with srilankite structure, ZrO_2 with tetragonally distorted fluorite structure), the higher are the Avrami exponents. The maximum values of about 4 correspond to a crystallization mechanism of a constant nucleation rate with subsequent three-dimensional crystallite growth. When the growth is disturbed, the Avrami exponent is reduced more or less.

From the ordinate intercept b and the apparent activation energies E'_a of the Kissinger plots, the apparent preexponential factors $c_0'\approx(p_0'k_0^m)^{1/n}$ can be calculated according to eqn. (5). They show a strong increase with increasing values of E_a'. A similar trend was observed for the thermally activated diffusion in amorphous alloys.[33–35] The plot of the logarithm of the Arrhenius preexponential factors *versus* the diffusion activation energies of several iron–zirconium alloys, shown in ref. 33, exhibits a linear correlation approximately. This relation can be deduced from the Eyring theory, which yields a temperature dependence of the rate constants of

$$c=\frac{kT}{h}\exp(\Delta S^{\neq}/R)\exp(\Delta H^{\neq}/RT) \qquad (8)$$

instead of the Arrhenius law.[36] For a small temperature range, the frequency factor kT/h is approximately constant, and the Arrhenius preexponential factor c_0 can be identified as

$$c_0=\frac{kT}{h}\exp(\Delta S^{\neq}/R) \qquad (9)$$

containing the activation entropy $\Delta S^{\ddagger}$. The Arrhenius activation energy E_a corresponds to the activation enthalpy $\Delta H^{\ddagger}$. In contrast to gas reactions, usually $\Delta S^{\ddagger}$ is positive in the solid state, because the transition state requires a high mobility to enable a reorientation of the fragments into another structure. The increase of the activation energies E_a and activation enthalpies $\Delta H^{\ddagger}$ observed in refs. 33–35 was attributed to a larger number of atoms involved in a collective motion during a diffusion step. This is accompanied with an increase of the activation entropy $\Delta S^{\ddagger}$. In case of an approxi-

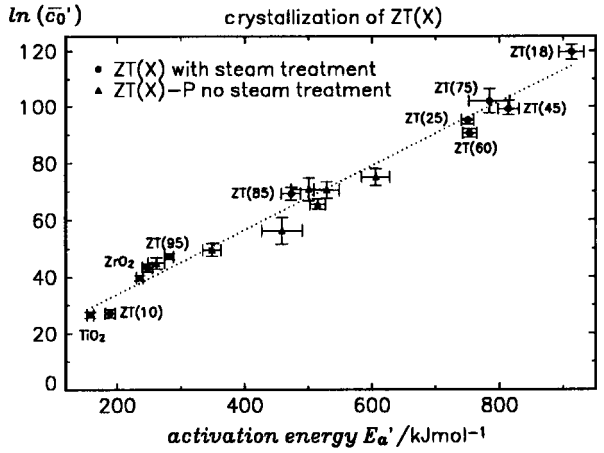

Fig. 5 Logarithmic plot of the Arrhenius preexponential factor c'_0 *versus* activation energy E'_α for the samples $Zr_xTi_{1-x}O_2$ [ZT(X) with $X = 100x = ZrO_2$ content in %], with standard deviation calculated from the linear regression.

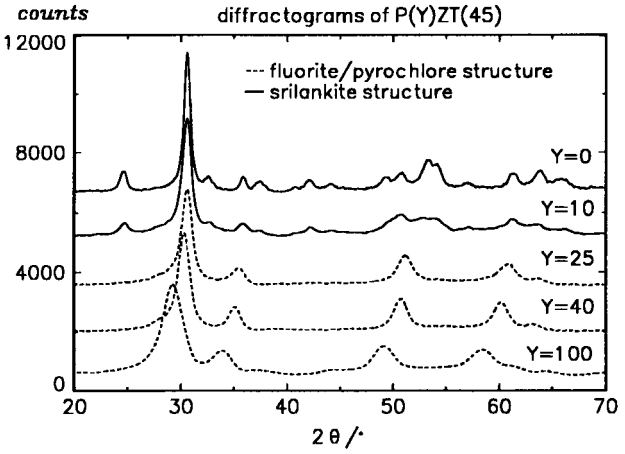

Fig. 6 Diffractograms of $Pb_yZr_{0.45}Ti_{0.55}O_{2+y}$ [P(Y)ZT(45) with $Y = 100y$ = PbO content in %], shifted along the ordinate for clarity.

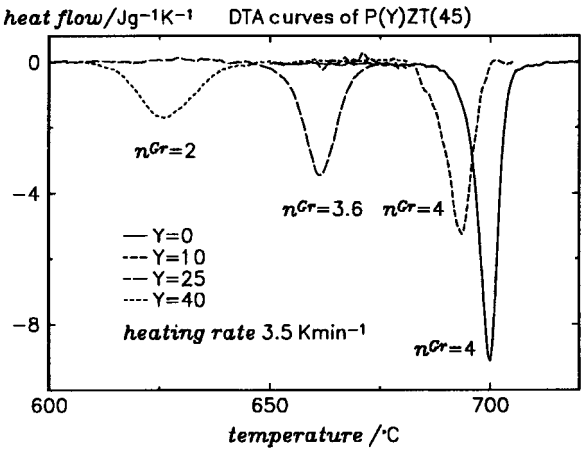

Fig. 7 Differential thermal analysis curves of $Pb_yZr_{0.45}Ti_{0.55}O_{2+y}$ [P(Y)ZT(45) with $Y = 100y$ = PbO content in %], prepared in 2-methoxyethanol with steam treatment.

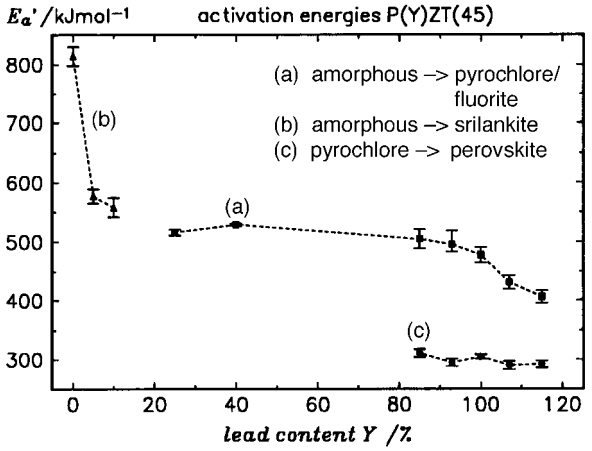

Fig. 8 Apparent activation energies of $Pb_yZr_{0.45}Ti_{0.55}O_{2+y}$ [P(Y)ZT(45) with $Y = 100y$ = PbO content in %], prepared in 2-methoxyethanol with steam treatment, with standard deviation calculated from the linear regression.

mate proportionality $\Delta S^\ddagger \sim \Delta H^\ddagger$, we get from eqn. (9) the observed linear relation $\ln c_0 \sim \Delta S^\ddagger \rightarrow \ln c_0 \sim \Delta H^\ddagger$.

This interpretation of the Arrhenius preexponential factors can be transferred to the crystallization of the ZT(X) samples. The increase of E_a' can be attributed to a larger number of (Zr/Ti)—O—(Zr/Ti) bonds which must be broken in the transition state, and therefore $E_a' \sim \Delta S^\ddagger$ can be assumed. In Fig. 5 the plot of ln c_0' *versus* E_a' is shown, which clearly exhibits a linear relation between these quantities. The maximum effect of the activation entropy on c_0' can be estimated from the crystallization of ZT(18) taking place at about 650 °C. From $c_0' \approx 10^{52}$ min^{-1} and $kT/h \approx 10^{15}$ min^{-1}, we get $\Delta S^\ddagger \approx 700$ J mol^{-1} K^{-1} which is still below the entropy of sublimation of about 765 J mol^{-1} K^{-1} estimated from the sublimation enthalpy of TiO_2.

Another example of the correlation of activation energies and Arrhenius preexponential factors can be found in ref. 37 for the crystallization of $PbTiO_3$. For samples prepared by coprecipitation or sol–gel processing, activation energies of 260–270 kJ mol^{-1} and preexponential factors of 2×10^{15}–7×10^{17} s^{-1} were determined. Amorphous $PbTiO_3$, prepared from the melt by roller quenching, yields $E_a' =$ 633 kJ mol^{-1} and $c_0' = 4 \times 10^{37}$ s^{-1}. The higher activation energy of the roller quenched sample can be attributed to the stronger hindrance of movements due to the significantly higher density. The collective motion of the adjacent (Zr/Ti)O_6 octahedra increases $\Delta S^\ddagger$ and therefore also c_0'.

5 Solid solution series P(Y)ZT(45)

The samples P(Y)ZT(45), prepared in MOE with steam treatment, can be examined over the whole range $0 \leqslant Y \leqslant 100\%$, and additionally even with a lead excess ($y =$ 107% and $y = 115\%$). P(5)ZT(45) and P(10)ZT(45) crystallize in the srilankite structure. At larger PbO contents, the samples form the fluorite structure with a continuous transition to the pyrochlore phase. The diffractograms are shown in Fig. 6. The crystallite size decreases from 350 Å [ZT(45)] and 160 Å [P(10)ZT(45)] to 110 Å [P(40)ZT(45)] and down to 40 Å for the pyrochlore phase of P(85)ZT(45)–P(115)ZT(45).

In Fig. 7 the DTA curves of ZT(45)–P(40)ZT(45) are depicted. With increasing PbO content, the crystallization temperature decreases and the peaks broaden. The apparent activation energies are shown in Fig. 8. A PbO content of 5% already reduces E_a' from 800 kJ mol^{-1} to below 600 kJ mol^{-1} without changing the crystal structure. E_a' of the formation of the fluorite or pyrochlore phase is constant at about 530 kJ mol^{-1} for P(10)ZT(45)–P(100)ZT(45) and slightly decreases with an excess of PbO to 420 kJ mol^{-1} for P(115)ZT(45). The transformation of the pyrochlore phase to the perovskite phase, which can be observed for the samples P(85)ZT(45)–P(115)ZT(45), has a constant activation energy of 300 kJ mol^{-1}. The crystallization enthalpy decreases strongly from 16 kJ mol^{-1} for ZT(45) to 8 kJ mol^{-1} for

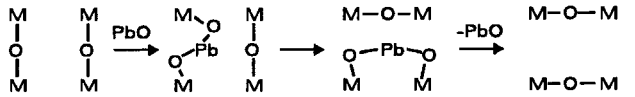

Fig. 9 Schematic representation of the (Zr/Ti)—O—(Zr/Ti) bond reconstruction in the presence of PbO. M = (Zr/Ti).

P(40)ZT(45) and to only 3 kJ mol^{-1} for the pyrochlore formation of PZT(45).

The Avrami exponents n^{Gr} decrease parallel to the decrease of the crystallite size from about 4 for ZT(45)–P(10)ZT(45) to 2 for P(40)ZT(45) and about 1.5 for P(85)ZT(45)–P(115)ZT(45). The small n^{Gr} for the pyrochlore formation of P(85)ZT(45)–P(115)ZT(45) can be interpreted with a high, constant nucleation rate and subsequent growth to a maximal crystallite radius of 20 Å.[21] Growth to larger maximal radii corresponding to the crystallite sizes found for P(40)ZT(45) and P(25)ZT(45) yields Avrami exponents closer to 4.

The decrease of E_a' and thus E_n and E_g can be explained by the involvement of PbO in the reconstruction of the $(Zr/Ti)O_6$ network. Lead has a high mobility either in the form of PbO (*cf.* the high vapour pressure of PbO[38]) or in the form of Pb^{2+} (*cf.* the high diffusion coefficient of Pb^{2+} in sintered $ZrTiO_4$[39]). A small amount of lead is sufficient to act as a 'catalyst' and to break many bonds subsequently. The decrease of the activation energy can interpreted by the avoiding of energetically unfavourable fragments during crystallization. The effect of PbO is shown schematically in Fig. 9. The insertion of PbO into a O—(Zr/Ti)—O—(Zr/Ti)—O bond is energetically more favourable than the formation of O—(Zr/Ti)—$\underline{O}|$+(Zr/Ti)—O fragments which is required in the absence of lead. The Pb—O bonds, which are weaker compared to (Zr/Ti)—O bonds, can be broken easily. The additional oxygen atom, introduced with the PbO, ensures that the Zr/Ti atoms are surrounded by at least 6 oxygen atoms during the rearrangement of the $(Zr/Ti)O_6$ network. Thus the unfavourable (Zr/Ti)—O fragments with a reduced coordination number are avoided. After the rearrangement, the PbO is eliminated again, leaving the modified $(Zr/Ti)O_6$ network. The decrease of the crystallite sizes with increasing lead content can also be explained by this model. If the PbO is not eliminated, then a configuration (Zr/Ti)—O—Pb—O—(Zr/Ti) remains. Owing to mechanical stress caused by the volume shrinkage during crystallization, the weaker Pb—O bonds can be broken yielding (Zr/Ti)—O—Pb+$|\underline{O}$—(Zr/Ti). The continuous octahedral network is broken and thus the crystallite growth is stopped.

The pyrochlore phase of PZT(45) is the lead rich end member of this solid solution series. Therefore the small crystallite size of 40 Å, the Avrami exponent of 1.5 and the apparent activation energy of 500 kJ mol^{-1} (which is relatively high compared with $E_a' \approx 300$ kJ mol^{-1} for the pyrochlore to perovskite transformation[21]) are not exceptional.

6 Solid solution series P(Y)T

The samples P(Y)T-P with $0 \leqslant Y \leqslant 15\%$ crystallize in the anatase structure. The reflections are only slightly broadened, indicating a crystallite size of more than 600 Å for all samples. The DTA curves of these samples are depicted in Fig. 10. The DTA peaks are shifted to higher temperatures and strongly broadened with increasing PbO content. Correspondingly, the Avrami exponents n^{Gr} decrease from 4 for TiO_2-P to 1.5 for P(15)T-P. The apparent activation energies from the Kissinger plots are about 260 kJ mol^{-1}, and the crystallization enthalpies are about 18 kJ mol^{-1}. Both energies are independent of the PbO content.

The lowering of the Avrami exponents for P(5)T-P–P(15)T-P can be explained by a mechanism of a constant nucleation rate and subsequent crystallite growth which is more or less hindered. When the crystallite growth ceases at some large (>1000 Å) but fixed radius, n decreases without any effect on the XRD line width. This is observed, *e.g.*, for the perovskite formation of PZT in ref. 21. In order to explain the large shifts of the crystallization temperatures with increasing PbO content, a corresponding decrease of the Arrhenius pre-exponential factors p_0 and k_0 must also be assumed. In total, the presence of PbO in TiO_2 gels seems to hinder the crystallization.

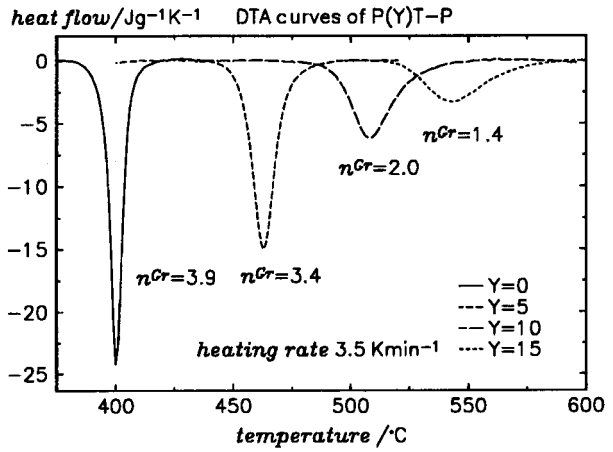

Fig. 10 Differential thermal analysis curves of Pb_yTiO_{2+y} [P(Y)T-P with $Y = 100y$ = PbO content in %], prepared in *n*-propanol without steam treatment.

7 Solid solution series P(Y)Z

The samples P(Y)Z, prepared in MOE with steam treatment with a PbO content of $0 \leqslant Y \leqslant 10\%$, crystallize in the tetragonally distorted fluorite structure. The crystallite size decreases from over 1000 Å for ZrO_2 to about 500 Å for P(5)Z and P(10)Z. The DTA peak temperatures at a heating rate of $\alpha = 3.5$ K min^{-1} shift from 380 °C for ZrO_2 to 425 °C for P(5)Z and to 455 °C for P(10)Z. All the Avrami exponents n^{Gr} have values larger than 4 due to overheating, even after mixing with Al_2O_3. The apparent activation energies are constant at about 270 kJ mol^{-1}, and the crystallization enthalpies are about 19 kJ mol^{-1}.

The effect of the presence of PbO in ZrO_2 gels is similar to that observed for P(Y)T-P. The activation energies of TiO_2 and ZrO_2 are already so low that no further decrease occurs when lead is added. It can be assumed that (Zr/Ti)—O—Pb—O—(Zr/Ti) bonds are also formed in these systems, and that they can be broken easily to (Zr/Ti)—O—Pb+$|\underline{O}$—(Zr/Ti), which stops the crystallite growth. Thus the crystallization is hindered by the lead addition, which is detectable in an increase of the crystallization temperatures and a decrease of the Avrami exponents and crystallite sizes.

8 Summary

In the solid solution series of ZT(X), extremely high apparent activation energies, reaching the values of the sublimation enthalpies of ZrO_2 and TiO_2, are found for intermediate ZrO_2 contents of 18–75%. The most plausible explanation is the favoured formation of Zr—O—Ti bonds during the gel formation. These bonds are broken with a preferred direction yielding the fragments Ti—$\underline{O}|$+Zr, and thus it may be necessary to break additional bonds of a $(Zr/Ti)O_6$ octahedron to form the fragments required for the continuation of the crystallite growth. Therefore the activation energy is increased

strongly. A linear relation between the logarithm ln c_0' of the apparent Arrhenius preexponential factor and the apparent activation energy E_a' is found. It can be explained by the contribution of the activation entropy $\Delta S^{\ddagger}$ which is increased parallel to the number of broken bonds and E_a'.

The incorporation of lead in the amorphous pyrolyzed gels of P(Y)ZT(X) hinders the crystallite growth, which is manifested either in a decrease of the Avrami exponent or in XRD line broadening, or both. In the samples where the corresponding ZT(X) exhibits a large apparent activation energy, E_a' is lowered drastically by the addition of lead and thus the crystallization is accelerated. The reduction of E_a' can be explained by the stabilization of the fragments formed from (Zr/Ti)—O—(Zr/Ti) bonds by interaction with PbO. For samples where the corresponding ZT(X) already has a low value of E_a', the lead addition does not alter the activation energy, but the DTA peak temperatures are shifted strongly to higher temperatures upon lead addition. Here the hindrance of the crystallite growth is the main effect of the PbO.

Notes and references

1 C. D. E. Lakeman and D. A. Payne, *Mater. Chem. Phys.*, 1994, **38**, 305.
2 J. Gopalakrishnan, *Mater. Chem.*, 1995, **7**, 1265.
3 E. A. Barringer and H. K. Bowen, *Langmuir*, 1985, **1**, 414.
4 M. T. Harris and C. H. Byers, *J. Non-Cryst. Solids*, 1988, **103**, 49.
5 P. M. Smit, A. Van Zyl and A. I. Kingon, *Mater. Chem. Phys.*, 1987, **17**, 507.
6 O. Yamaguchi, T. Fukuoka and Y. Kawakami, *J. Mater. Sci. Lett.*, 1990, **9**, 958.
7 R. Merkle and H. Bertagnolli, *J. Mater. Sci.*, 1998, in press.
8 P. Debye and H. Menke, *Phys. Z.*, 1930, **31**, 797.
9 K. A. Kerr and J. P. Ashmore, *Acta Crystallogr., Sect. A*, 1974, **30**, 176.
10 P. Scherrer, *Gött. Nachr.*, 1918, **2**, 98.
11 H. P. Klug and L. E. Alexander, *X-ray Diffraction Procedures for Polycrystalline and Amorphous Materials*, Wiley and Sons, New York, 2nd edn., 1974.
12 W. A. Johnson and R. F. Mehl, *Trans. Am. Inst. Min. Eng.*, 1939, **135**, 416.
13 M. Avrami, *J. Chem. Phys.*, 1939, **7**, 1103.
14 M. Avrami, *J. Chem. Phys.*, 1940, **8**, 213.
15 M. Avrami, *J. Chem. Phys.*, 1941, **9**, 177.
16 H. E. Kissinger, *Anal. Chem.*, 1957, **29**, 1703.
17 J. W. Graydon, S. J. Thorpe and D. W. Kirk, *Acta Metall. Mater.*, 1994, **42**, 3163.
18 J. W. Cahn, *Acta Metall.*, 1956, **4**, 572.
19 D. W. Henderson, *J. Non-Cryst. Solids*, 1979, **30**, 301.
20 J. W. Graydon, S. J. Thorpe and D. W. Kirk, *J. Non-Cryst. Solids*, 1994, **175**, 31.
21 R. Merkle and H. Bertagnolli, *Ber. Bunsenges. Phys. Chem.*, 1998, **102**, 1023.
22 I. Manzini, G. Antoniolo, D. Bersani, P. P. Lottici, G. Gnappi and A. Montanero, *J. Non-Cryst. Solids*, 1995, **192–193**, 519.
23 Bokhimi, A. Morales, O. Novaro, T. Lopez, E. Sanchez and R. Gomez, *J. Mater. Res.*, 1995, **10**, 2788.
24 K. Terabe, K. Kato, H. Miyazaki, S. Yamaguchi, A. Imai and Y. Iguchi, *J. Mater. Sci.*, 1994, **29**, 1617.
25 O. Yamaguchi and H. Mogi, *J. Am. Ceram. Soc.*, 1989, **72**, 1065.
26 A. E. McHale and R. S. Roth, *J. Am. Ceram. Soc.*, 1986, **69**, 827.
27 P. Colomban and E. Bruneton, *J. Non-Cryst. Solids*, 1992, **147–148**, 201.
28 G. H. Aylward and T. J. H. Findlay, *SI Chemical Data*, J. Wiley & Sons, New York, 2nd edn., 1974.
29 D. C. Bradley, R. Gaze and W. Wardlaw, *J. Chem. Soc.*, 1955, 3977.
30 D. C. Bradley, R. Gaze and W. Wardlaw, *J. Chem. Soc.*, 1957, 469.
31 D. C. Bradley and D. G. Carter, *Can. J. Chem.*, 1961, **39**, 1434.
32 R. Ahlfänger, H. Bertagnolli, T. Ertel, U. Kolb, D. Peter, R. Naß and H. Schmidt, *Ber. Bunsenges. Phys. Chem.*, 1991, **95**, 1286.
33 W. Frank, U. Hamlescher, H. Kronmüller, P. Scharwaechter and T. Schuler, *Phys. Scr.*, 1996, **T66**, 201.
34 W. Frank, A. Hörner, P. Scharwaechter and H. Kronmüller, *Mater. Sci. Eng. A*, 1994, **179/180**, 36.
35 B. Damson and R. Würschum, *J. Appl. Phys.*, 1996, **80**, 747.
36 R. W. Cahn and P. Haasen, *Physical Metallurgy*, North Holland Publications, Amsterdam, 1983.
37 R. W. Schwartz and D. Payne, *Mater. Res. Soc. Symp. Proc.: Better Ceramics through Chemistry III*, 1988, **121**, 199.
38 K. H. Härdtl and H. Rau, *Solid State Commun.*, 1969, **7**, 41.
39 M. V. Slinkina and G. I. Dontsov, *Inorg. Mater.*, 1992, **28**, 429.

Paper 8/04552F